LUND UNIVERSITY

Light sheet fluorescence microscopic imaging for high-resolution visualization of spray dynamics

Berrocal, Edouard; Kristensson, Elias; Zigan, Lars

Light sheet fluorescence microscopic imaging for high-resolution visualization of spray dynamics

Edouard Berrocal[1,2], Elias Kristensson[1] and Lars Zigan[2,3]

Abstract

In this study, the use of light sheet fluorescence microscopic imaging is demonstrated for viewing the dynamic of atomizing sprays with high contrast and resolution. The technique presents several advantages. First, liquid fluorescence gives a more faithful representation of the structure of liquid bodies, droplets, and ligaments than Mie scattering does. The reason for this is that the signal is emitted by the fluorescing dye molecules inside the liquid itself and not generated at the air–liquid interfaces. Second, despite the short depth of field ($\sim$200 μm) obtained when using the long range microscope, the contribution of out-of-focus light is much smaller on a light sheet configuration than for line-of-sight detection, thus providing more clearly sectioned images. Finally, by positioning the light sheet on the spray periphery, toward the camera objective, the effects due to multiple light scattering phenomena can be reduced to some extent. All these features provide, for many spray situations, good fidelity images of the liquid fluid, allowing the extraction of the velocity vectors at the liquid boundaries. Here, double frame images were recorded with a sCMOS camera with a time delay of 5 μs between exposures. A typical pressure-swirl atomizer is used producing a water hollow-cone spray, which was imaged in the near-nozzle region and further downstream for injection pressures between 20 bar and 100 bar. Furthermore, near-nozzle spray shape visualization of a direct-injection spark ignition injector was conducted, describing the disintegration of the liquid fuel and droplet formation. Such data are important for the validation of computational fluid dynamics models simulating liquid breakups in the near-field spray region.

1. Introduction

Light sheet fluorescence microscopy (LSFM) has become, during the past decade, one of the largest growing techniques in optical microscopy.[1–3] This interest has led to publications in high impact factor journals and the approach has been selected "Method of the year 2014" by Nature Methods.[4] Despite all those recent recognitions in the field of life science microscopy, it should be reminded that laser sheet fluorescence imaging was already reported for macroscopic imaging more than 30 years ago by Melton and Verdieck[5] for spray visualization.[5] This first attempt for studying sprays was applied in a hollow cone fuel spray. The spray was irradiated with a sheet of UV laser light, and with appropriate filters, two-dimensional sections of the liquid and vapor fluorescence of the evaporating

spray were separately photographed. The separation of the liquid and gas phase was performed by means of laser-induced exciplex fluorescence (LIEF). From this publication, it can be noticed that the resultant images were blurred due to the detection of multiple light

[1]Division of Combustion Physics, Department of Physics, Lund University, Lund, Sweden
[2]Erlangen Graduate School in Advanced Optical Technologies (SAOT), Universität Erlangen-Nürnberg, Germany
[3]Lehrstuhl für Technische Thermodynamik (LTT), Universität Erlangen-Nürnberg, Germany

Corresponding author:
Edouard Berrocal, Division of Combustion Physics, Department of Physics, Lund University, Lund, Sweden.
Email: edouard.berrocal@forbrf.lth.se

scattering. The authors already mentioned this problem related to the spray optical density, stating: "As long as the spray is optically thin, the fluorescence from a droplet is proportional to its mass". To face issues related to the contribution of multiple light scattering intensities structured laser illumination planar imaging (SLIPI) technique was co-developed by Berrocal et al.[6] and Kristensson et al.[7] in 2008, showing high contrast macroscopic images of the spray structure of a hollow-cone water spray running at 50 bar pressure of injection. The technique was then further applied for both three-dimensional reconstruction of the spray region[8,9] and single-shot Mie imaging of the near-nozzle region.[10,11]

Microscopic imaging is of strong interest for spray analysis, as the atomization process produces liquid structures and ligaments on the order of hundreds of microns, and droplets size ranging from only a few to several tenths of microns. However, the transition from macroscopic to microscopic imaging is challenging for spray systems. In opposition to biological or medical samples, where a microscope objective can be placed very close to the sample, the same is not possible for spray systems as the droplets would impinge on the collecting lens. In addition, if the spray is studied at high pressure and/or temperature conditions within an optical chamber, then the minimum distance between the spray and the objective usually fall within the order of a half to one meter. Basic magnification strategies based on adding a number of extension rings are not ideal, usually leading to significant image distortion due to artefacts from spherical and chromatic aberrations. Therefore, the objective must be diffraction-limited and this over the entire field of the camera sensor to obtain the optimum clarity and resolution throughout the imaged field. Such requirements have been recently satisfied by the development of high-performance long-distance microscope objectives such as the ones developed by "Infinity Photo-Optical Company" (e.g. K-series long-distance microscopes). Thanks to such objectives, microscopic shadowgraphy imaging has already been well applied for the study of diesel sprays by Crua et al.[12–14] Despite using a long-distance microscope, which provides very short depth of field (~200 μm), thus providing a section of the spray, the main limitation concerns the fact that this does not remove the detection of out-of-focus light. This effect is typical of line-of-sight imaging and also occurs for a backscattering detection. By instead using a light sheet of width equal to the depth of field of the camera microscopic objective, the illumination itself optically sections the spray, strongly reducing the collection of out-of-focus light. By also positioning the light sheet at a desired location on the spray periphery, the amount of induced multiple light scattering between

the light sheet and the camera can somehow be controlled, allowing to extract valuable information on liquid breakups on the spray periphery even under challenging situations.

In this article, we present, to the best of the authors' knowledge, one of the first applications of LSFM for spray diagnostics. A comparison of the technique with other imaging configuration is first given, to highlight the advantages of LSFM. Then the technique is applied in a hollow cone spray generated by a pressure swirl atomizer running between 20 bars and 100 bars water pressure of injection. To observe the time evolution of the liquid structures near the nozzle tip, series of two images have been recorded with 5 μs time duration between exposures. Droplet sizing was conducted using LSFM 120 mm downstream from the injector tip. Furthermore, a study of the near-nozzle jet disintegration of a DISI-injector has been conducted using microscopic laser-induced fluorescence (LIF) and Mie scattering in an injection chamber at IC engine-relevant conditions.

2. Material and methods

2.1. LSFM in a hollow-cone spray

The spray investigated in this article is a steady state (continuously running) hollow-cone water spray of 60° full spray angle, created using a pressure swirl nozzle of 1 mm orifice diameter (Lechler, ordering no. 216.324). It is illuminated from two successive laser pulses of 10 ns pulse duration, generated from two Nd:YAG lasers emitting at 532 nm wavelength. The two laser beams, which are crossed polarized, are spatially recombined using a polarizer beam splitter. The spray is imaged at 90° using a long-range microscope objective, Model K2 DistaMax, mounted on a sCMOS LaVision camera (2560 × 2160 pixels). The field of view is in the range of 6 mm × 5 mm resulting into 2.3 μm in pixel resolution.

The time delay between the two exposures is fixed to 5 μs and images are recorded using the double frame mode of the camera. A laser sheet of 6 mm in height is formed with an adjustable slit allowing fixing its width as desired (in this case ~300 μm). This way, the thickness of the light sheet can be accurately adjusted to match the depth of field of the long distance microscope objective. Note that using light sheets narrower than the imaged liquid structures can lead to "cutting effects" of those structures. This is particularly true at low injection pressure where large ligaments are generated. The spray is running at room temperature and atmospheric pressure conditions. The injection pressure is varied from 20 to 100 bar with steps of 20 bar. The injected water is seeded with a translucent organic dye,

Eosine Y (Xanthene derivative), which is characterized by a quantum yield of 0.36 when mixed with water and 0.68 when mixed with ethanol according to Zhang et al.[15] It should be noted that ethanol is applied as fuel in the DISI-spray study. Ethanol is a worldwide commonly used biofuel for spark-ignition engines and thus, suitable fuel tracers for ethanol as solvent are of high interest for spray characterization using tracer laser-induced fluorescence. Especially in the liquid phase, typical fuel tracers such as 3-pentanone[16] or triethylamine[17] show very low fluorescence signal intensity in combination with ethanol. This effect is explained by intermolecular processes due to the hydrogen bonding between ethanol and the fuel tracer occurring in the liquid phase,[17] which is not the case for typical alkane model fuels such as iso-octane or n-heptane. Care should be taken for selecting an appropriate dye for the LIF studies as the signal is not only dependent on the concentration of the dye but it can be also influenced by temperature and laser fluence.

The fluorescence emission spectrum peaks at 550 nm when excited at 532 nm. A 532 nm notch filter with optical density 6 blocking is fixed on the camera objective to reject the Mie-scattered light from the excitation source. Due to the short depth of field of the long range microscope ($\sim$200 μm) and the conical structure of the spray, a large part of the spray was out-of-focus. To solve this issue, the injector has been rotated by $\sim$30° angle in order to have the periphery of the spray aligned vertically with the light sheet. This is shown on the photographs in Figure 2.

To illustrate the effects of multiple scattering and the optical density of the probed spray at different liquid pressures of injection three photographs are as shown in Figure 3. Note that in the experiment describe above, the imaged part of the spray is located right after the nozzle tip. However, due to the tilt of the injector, the first 3 mm were hidden by the injector itself (see Figure 2). Thus, the imaged area corresponds to $\sim$3 to 8 mm below the nozzle orifice.

2.2. LSFM and Mie scattering in a DISI spray

In the DISI spray experiment, an injection chamber is used in which the injector is mounted. The spray chamber is operated with dry air at 0.2 MPa and 293 K representing an injection at high load engine operating
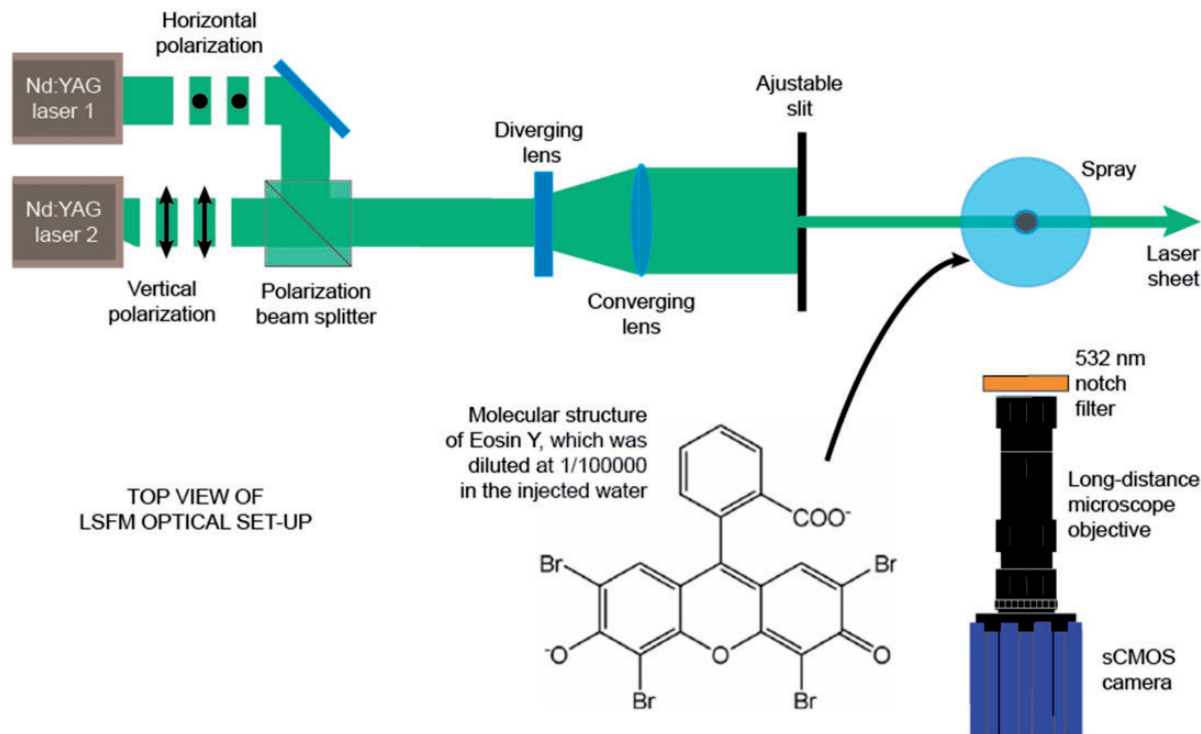
Figure 1. The optical arrangement with the long range microscope objective is shown on the left while the right image shows the illuminated area of the spray. The width of the light sheet is fixed to match the depth of field of the camera using an adjustable slit in front of the spray. The injector is tilted by 30° angle from the horizontal direction in order to keep a sharp image focus over the full field-of-view. Here, the spray is running at 40 bars pressure of injection.
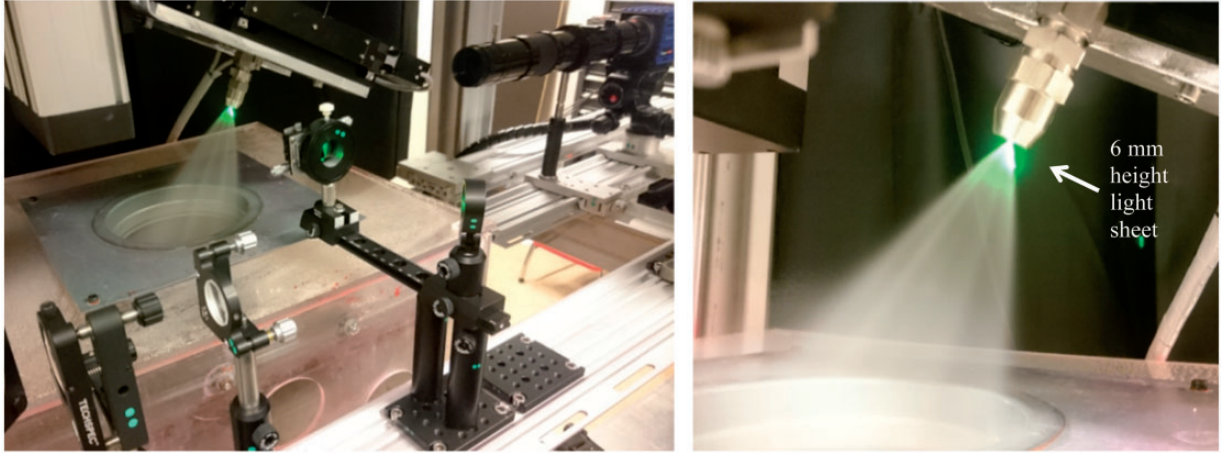
Figure 2. Schematic of the optical arrangement for light sheet fluorescence microscopy (LSFM). An adjustable slit has been used instead of a cylindrical lens to create a light sheet of desired thickness (slightly larger ~300 µm than the depth of field of the long-distance microscope objective). A too thin light sheet could optically cut some large liquid structured at low pressure of injection while a too large light sheet will contribute to undesired out-of-focus signal. A notch filter is used in front of the objective to reject the 532 nm contribution and collect the entire fluorescence signal. Eosin Y is mixed with the injected water to induce fluorescence.
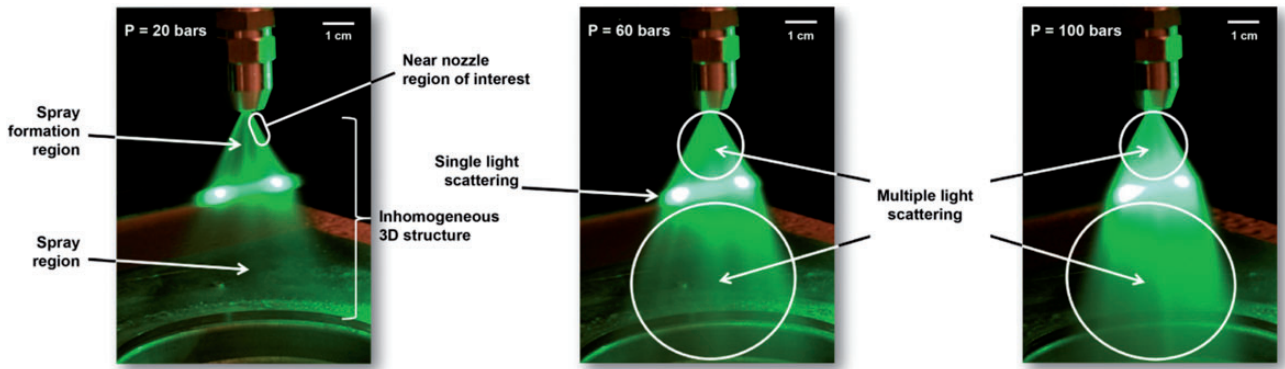
Figure 3. Occurrence of multiple light scattering when increasing the pressure of injection for the studied hollow cone water spray. In these illustrative photographs, a 532 nm CW laser beam is crossing the spray at 3 cm below the nozzle tip and the pressure of injection is increased from 20 to 100 bars. Note that for all presented results only the near-field region, at distance 3 to 8 mm below the nozzle orifice is imaged (as indicated on the left-side picture).

point. The injection duration is kept constant at 1800 µs and the injection repetition rate was 1 Hz. The injection pressure is set to 8 MPa. A 5-hole DISI injector (BOSCH) is utilized, where one jet is centrally separated from the others, which is studied using the microscopic LIF and Mie-scattering setup.

A macroscopic Mie-scattering image of the studied multi-jet spray is presented in

Figure 4 together with the optical setup used for microscopic spray imaging.

In this study, ethanol is used as fuel and again, the tracer eosin Y is added to the fuel for the laser-induced fluorescence studies. In principle, the same optical setup is used as for the water spray studies. However, the camera filters are replaced during the study to realize both a detection of the fluorescence (532 nm notch filter) and the Mie scattering (532 nm laser line pass filter). This enables a first differentiation of the image quality in terms of representation of the liquid spray shape for both imaging techniques. The height of the laser sheet is set to 8 mm and the laser power is ~20 mJ. Details of the injection system and spray chamber used can be found elsewhere.[18] The injector is described in more detail in Heldmann et al.[19]
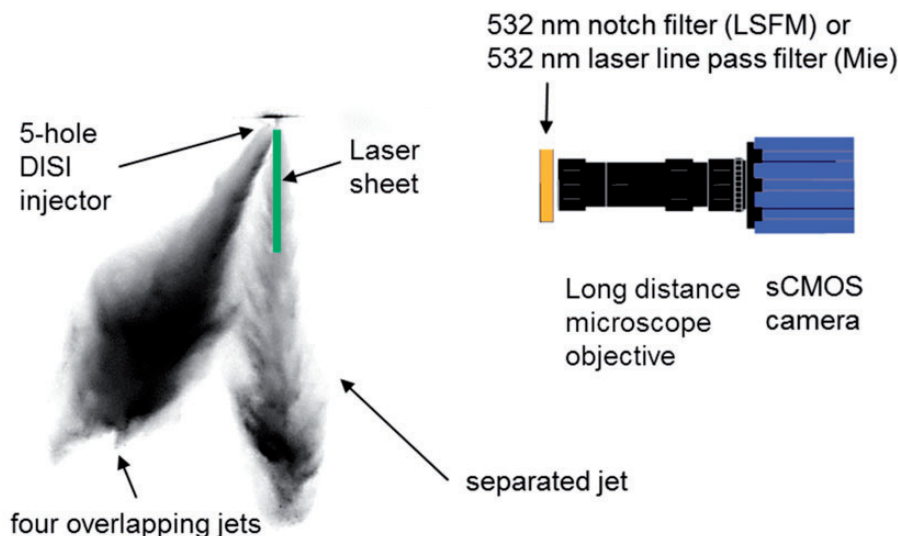
Figure 4. Schematic of the optical arrangement for light sheet fluorescence microscopy (LSFM) and microscopic Mie imaging in a DISI-spray generated by the 5-hole injector. A single-shot macroscopic Mie-scattering image (integral illumination using a flash lamp) shows the global spray evolution. Only one separated jet was studied whereas the four other jets are located in the background of the investigated plane. Size of camera and laser sheet are not to scale.

3. Comparison between LSFM and Mie-scattering microscopic imaging

### 3.1. Results for the hollow-cone steady spray

One important aspect of the work presented here is to determine the benefits of LSFM by comparing it with other optical configurations and detection schemes. In this section, we analyze the Mie-scattering detection by simply removing the notch filter in front of the camera shown in Figure 5 and by injecting water without adding any fluorescing dye. Note that here we define "Mie scattering" by the light being elastically scattered by any liquid elements present in the spray and not by the spherical droplets only.

While for macroscopic imaging of the spray region, Mie and LIF images usually appear quite similar (apart for the light intensity dependence to droplets surface for Mie and to droplets volume for LIF), this differs strongly in the case of microscopy where the irregular liquid elements are resolved. This observation is illustrated in Figure 5 where the spray was running under the exact same conditions for the Mie and LIF detections. For the Mie-scattering detection, parts of the spray are not even visible, especially at low pressure of injection where long irregular liquid elements are present (according to the LIF image). This can be explained by two reasons. First, the Mie scattering generates a signal only at each liquid–gas interfaces, where there is a change in refractive indices, but not inside the liquid structures themselves

(where the refractive index remains constant). Therefore, planar Mie images of highly atomizing spray will provide a more faithful representation of the spray than for poorly atomized sprays. This can be seen by increasing the pressure of injection up to 60 bars.

The second reason is that some of the irregular liquid elements directly reflect part of the incident light into the camera producing some light spots of very intense signal, reducing the camera dynamic range or directly saturating the camera sensor. As those intensity contributions originate from direct reflections, the corresponding light keeps most of the incident polarization. Therefore, one way to reduce those effects is to use a linear polarizer orientated in opposite direction than the incident polarization in front of the camera objective. This would increase the camera dynamic range but it will not correct for other artefacts induced by the nature of the Mie-scattered light.

In opposition to the Mie detection, the LSFM images reveal a more faithful representation of the spray structure. This can be explained by the fact that the collected signal does not only come from the liquid-air interfaces, but from the liquid structures themselves, which contain the dye molecule. Thus, the light, which is being refracted within the liquid structures, excites the dye molecules resulting to the glow of the entire illuminated liquid body. While the volumetric dependence of the signal might limit the dynamic range of the camera, this appears not to be as problematic as the effects induced by the strong Mie reflections.
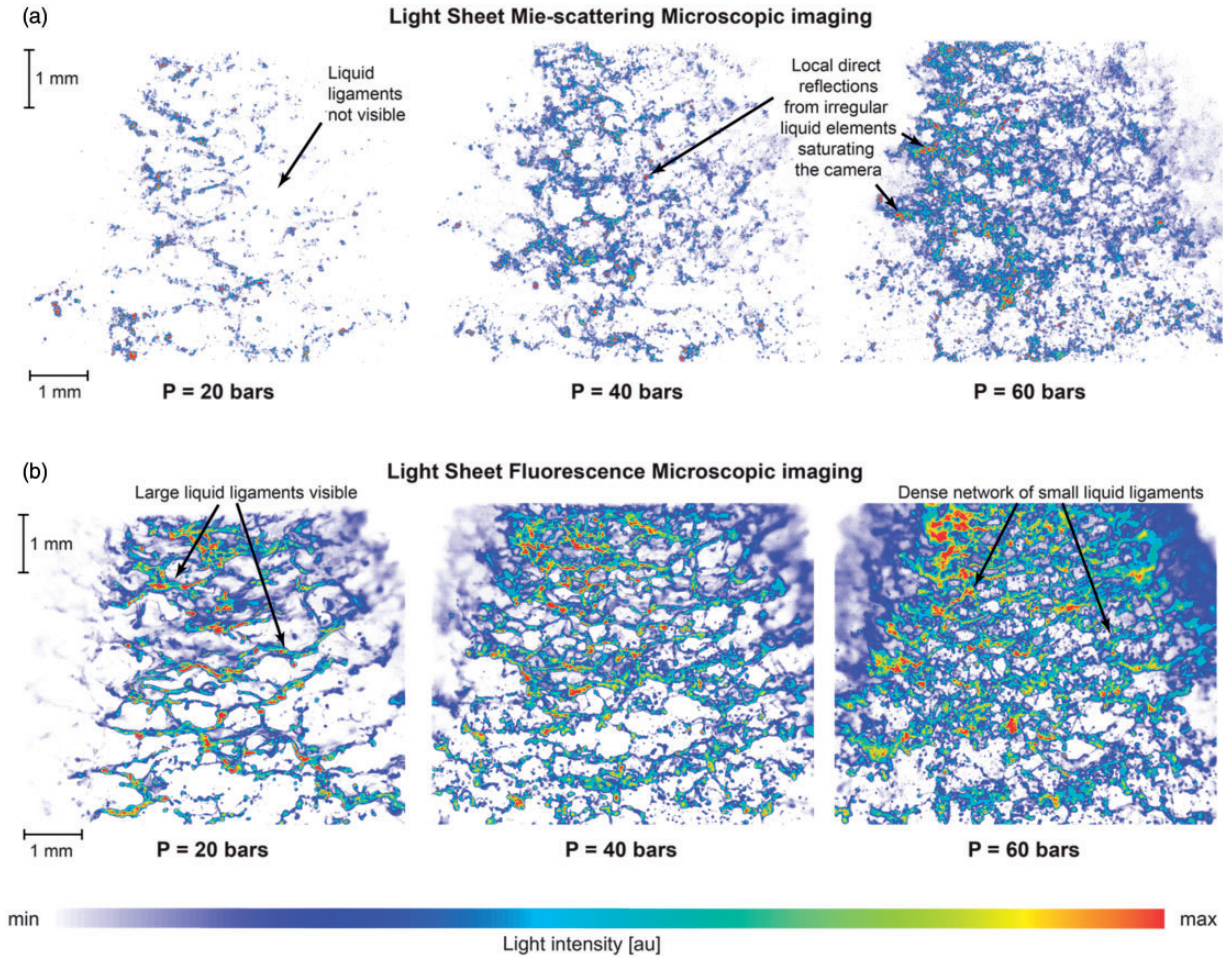
Figure 5. Comparison between light sheet Mie-scattering microscopic imaging (top row) and LSFM (bottom row). While the Mie-scattering images are lacking spray information and locally saturate the camera sensor, the LSFM images show a much more faithful representation of the spray structure.

3.2. Results for the transient DISI spray

In this section, the two microscopic planar imaging techniques are compared for its capability to faithfully analyze the spray structure of an IC engine spray, which characterized by very strong cyclic spray fluctuations due to the highly turbulent, unsteady nozzle flow.[19,20] First, the general spray structure is described that is resolved by the two different techniques in Figure 6. Afterwards, a statistic description will be provided in terms of average images and standard deviation of the signals (see Figure 7). In Figure 6, some examples of single-shot microscopic Mie scattering in (a) and LSFM images in (b) are presented for a DISI ethanol spray at 10 and 80 μs after visible start of injection.

Due to the high liquid density of the DISI spray at the nozzle exit, light is highly reflected at the liquid–air interfaces leading to very strong signal intensities, which locally saturate the camera for the Mie detection. In the same manner to the hollow-cone water spray, those direct reflections are enhanced by the collimated nature of the laser beam and are blocked for the LIF detection by the inserted notch filter. It could be added that those local saturations strongly reduce the dynamic of the camera. Thus, suppressing those effects is particularly advantageous. As a result, the LIF images present a better image dynamic despite the dependence of the signal with the volume of the fluorescing liquid. However, note that once the micrometric droplets are formed (i.e. at further downstream positions), those strong reflections are not occurring anymore, leading to a better image dynamic of the Mie images. This is because the Mie signal becomes related to the surface area of the droplets and not to their volume. In addition, extinction phenomenon occurs as light traverses the spray, giving a lower light intensity on the side where light exits the spray. This is observed for both
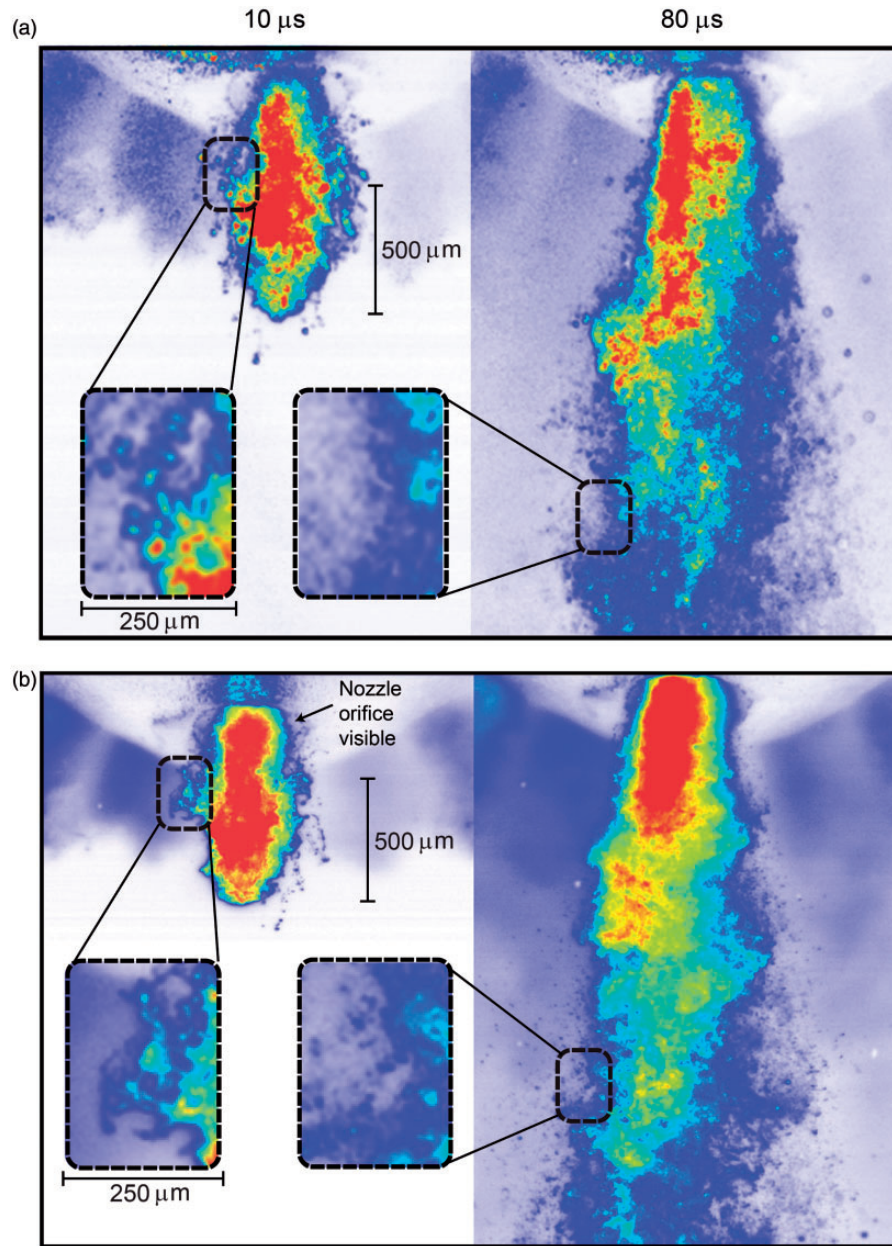
Figure 6. Comparison of microscopic images of a DISI spray injected at 80 bars pressure of injection taken at two different points in time during opening of the DISI injector (10 and 80 μs after the visible start of injection): In (a) examples of planar Mie-scattering images are shown. At 80 μs at the left spray boundary, the laser light is strongly scattered whereas the Mie-scattering signal is weak at the right spray boundary. In (b) LSFM images are presented. In both rows, illumination of the spray plume was conducted from the left hand side. High-resolution details of the liquid-gas interfaces are clearly visible together with the nozzle orifice.

the LIF and Mie-detection schemes. Finally, in the center of the spray, light interacts multiple times with the formed liquid bodies and droplets, blurring any spray information in this region. This is a phenomenon known as multiple light scattering. Thus, any definitive conclusion cannot be drawn, here, regarding the central region. However, on the spray periphery, faithful image information is obtained, as single light scattering is the dominant process. By comparing the zoomed areas, at

10 μs, it is seen that Mie-scattering image show some "granular" structures. Those structures are not physical and are an artefact induced by the illumination (collimated and coherent laser beam) and detection scheme (Mie scattering). Thus, they do not provide a correct representation of the spray structure. On the contrary, ligaments and inter-connected liquid bodies are visible on the zoomed fluorescence image. Thus, the LSFM image depicts more realistically the fluid mechanical process
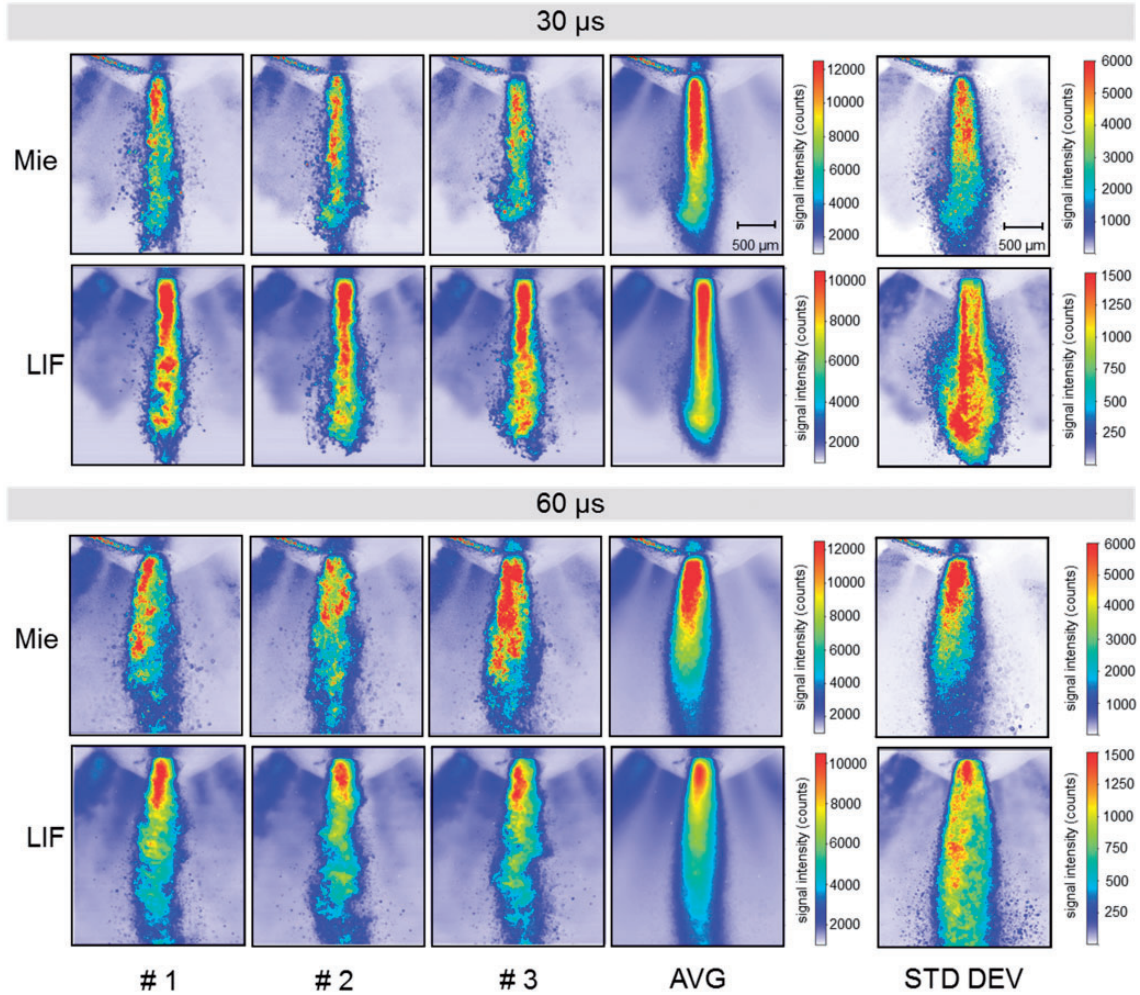
Figure 7. Microscopic images of a DISI spray injected taken at two different points in time during opening of the DISI injector (30 and 60 μs after the visible start of injection). Three examples of single shot images of planar Mie scattering and laser-induced fluorescence (LIF) are presented together with average images (AVG) and standard deviations (STD DEV). Please note that the subdivision of the color bars is different for the Mie and LIF images, esp. for the standard deviation (which is much larger for Mie scattering).

occurring in the spray. This is also confirmed in the zoomed area at 80 μs. In this case, the analysis of the small liquid bodies using Mie scattering is hardly possible, as the boundary of these ligaments and clusters appear blurred due to coherence effects. Thus, if one wants to obtain detailed analysis of the spray structure such as analyzing sizes of ligaments, clusters and large droplets (as shown in Zigan et al.[20]) by means of microscopic laser sheet imaging, it is recommended, to use liquid LIF instead of Mie-scattering detection.

For a more quantitative analysis, further statistical postprocessing of the images was conducted that is provided in Figure 7. Besides some additional single-shot images, also the average (AVG) and the standard deviation (STD DEV) is presented for both Mie-scattering images and LIF. Results for two points in time are provided (30 μs, 60 μs) at which the spray is already widely spread from the nozzle. The three single shot images show the cyclic variation of the spray in terms of spray lenght, cone angle and width and also some bending of the jet is visible. After averaging of the 30 individual images, the signal is more blurred and details of the spray structure cannot be resolved anymore. The larger dynamics of the fluorescence signal becomes very distinct in the single images but it is also apparent in the averaged images. Especially at the spray front region, the LIF intensity is much larger compared to the Mie signal, this can be also seen in the average image. It is very interesting that Mie-scattering and LIF images provide these distinct variations in spray structure even in the averaged images.

In the standard deviations, the differences due to the detection scheme are even larger. Of course, the standard deviation also provides information about the spray fluctuations from injection to injection, but again,

the general information should be comparable for both detection schemes. In general, the standard deviations are much larger for the Mie scattering (maximum is at 6000 counts) in comparison to LIF (maximum intensity is 1500 counts) while the absolute intensity is in the same range (maximum of 10,000 or 12,000 counts, respectively). The standard deviation is maximal for the first part of the spray (about 1 mm) and then it drops in the part of the spray front. This distribution is much more homogeneous for LIF, which is another

confirmation of its more accurate representation of the spray structure.

4. Comparison between LSFM and back-fluorescence microscopic imaging

4.1. Image comparison

In this sub-section, a comparison between back-fluorescence microscopic (BFM) imaging and LSFM
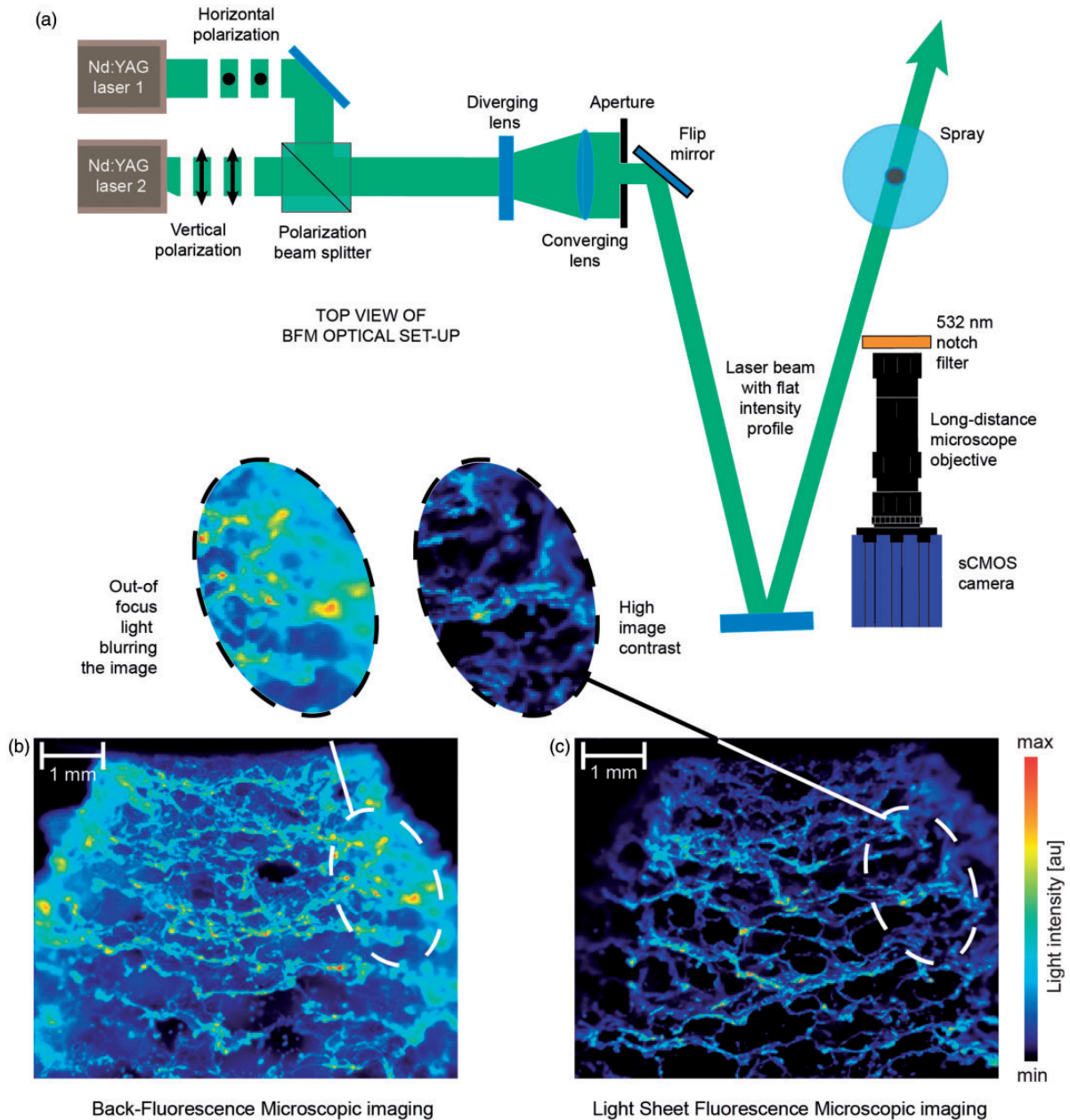
Figure 8. (a) Schematic of the optical arrangement for back-fluorescence microscopic (BFM) imaging. A flip mirror was used to switch in between the two optical arrangements, BFM and LSFM. (b) and (c) is the resulting image comparison between BFM and LSFM. It is seen that the contribution of out-of-focus light in BFM is reducing the image contrast, which is not the case for LSFM.
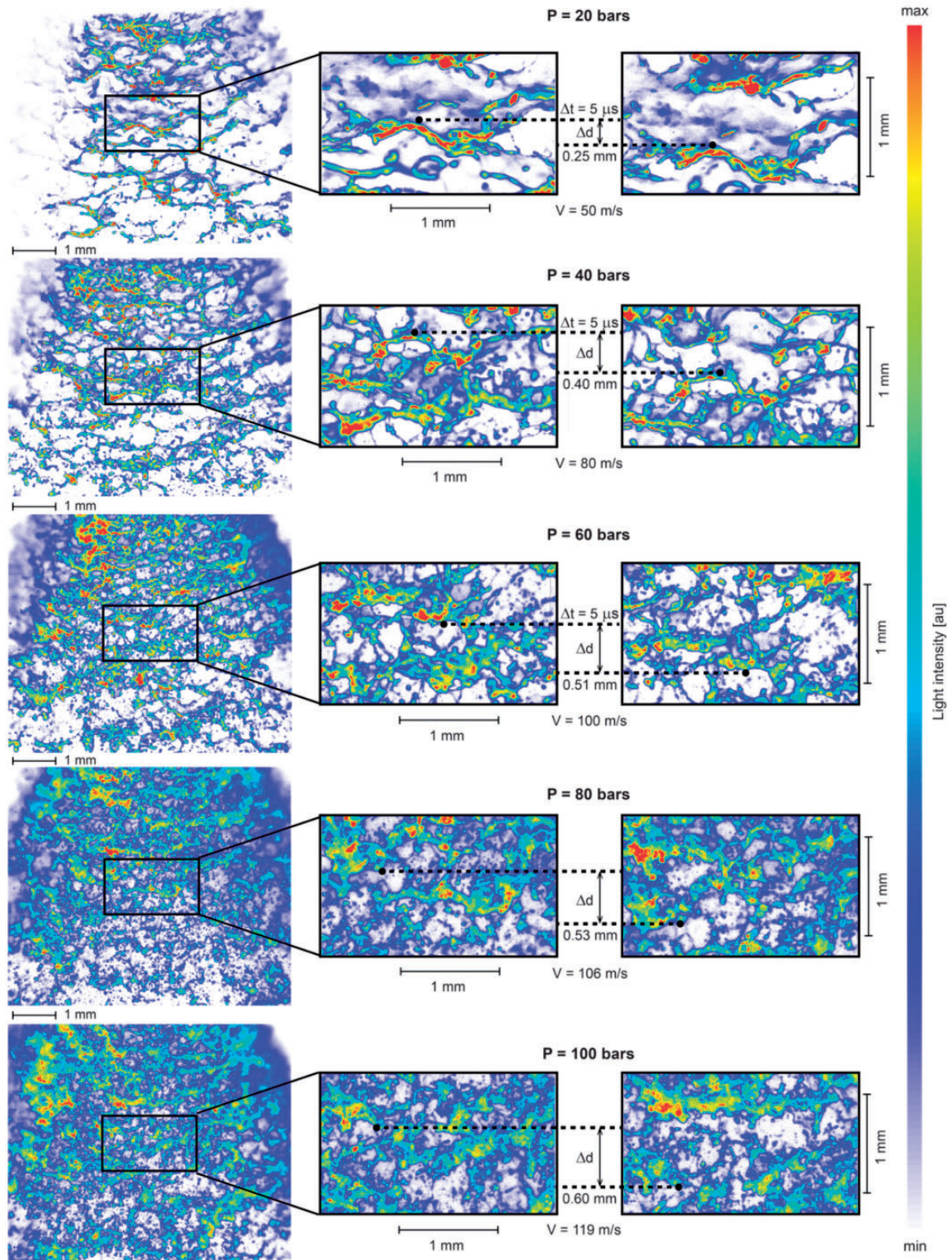
Figure 9. LSFM images of the liquid structures in the near-field region (between 3 and 8 mm below the nozzle tip) of a hollow-cone water spray. The water pressure of injection ranges between 20 and 100 bars. Zoomed views are shown on the right side where the displacement of liquid structures can be observed when applying a time delay of 5 µs between exposures. While at low water injection pressure the shape of liquid bodies remain identical between on the two exposures, this is not true anymore at high pressure of injections where the liquid structures are subjected to rapid deformations.

are shown for the hollow-cone water spray running at 30 bars pressure of injection. The spray was imaged with the same camera and long-distance microscope objective and running at identical conditions for both detection cases. The transition between the two optical configurations was quickly operated by means of a flip mirror. The optical arrangement of the back-fluorescence detection is shown in Figure 8(a). It is observed from Figure 8(b) and (c) that the image contrast is significantly enhanced with LSFM thanks to the reduction of out-of-focus light generated when using BFM. Those results demonstrate the sharp sectioning capabilities of LSFM, where a large amount of out of focus light is not generated.

4.2. LSFM for spray dynamics analysis

The LSFM images of the hollow-cone water spray, running from 20 bars to 100 bars pressure of injection, are shown in Figure 9. For each indicated injection pressure two magnified images are provided for a better visualization of the liquid structures. The time interval between in-between the two magnified images is 5 μs, allowing the observation of liquid displacement and deformation.

At 20 bar pressure of injection, large horizontal liquid filaments are observable below the nozzle tip. Even though the pressure of injection remains relatively low, there is no presence of a continuous liquid sheet, but rather of a network of interconnected ligaments. Those horizontal ligament/filaments can be over a millimeter long and ~100 μm in width. The strong fluorescence originating from those structures indicates that they are fairly thick (in the third dimension). After 5 μs, it is observed that those structures do not deform much and have a velocity in the range of 50 m/s.

At 40 bar and 60 bar pressure of injection a broadening of the ligaments in the vertical direction is apparent in comparison with the 20 bar case. However, the reduction in fluorescence intensity maxima indicates that those illuminated structures are of smaller volumes. Therefore, it is deduced that the liquid bodies are thinner in the third dimension and will be further responsible for the formation of smaller droplets. From the displacement of the liquid bodies within the indicated field of views it can be deduced that their velocities ranges around 80 m/s and 100 m/s, respectively. Even though some deformations are now visible on those structures, after 5 μs, liquid patterns can be easily recognized and tracked.

At 80 bar and 100 bar pressure of injection, the observed "liquid networks" do not appear as horizontal with the presence of less and smaller voids in the images. Once again, the detected fluorescent signal has reduced in comparison with the previous cases demonstrating the presence of even thinner liquid structures. The velocities of those liquid structures are ~105 m/s at 80 bar and ~120 m/s at 100 bar water injection pressure. In those cases, the deformations of the liquid bodies within the 5 μs time separation are really apparent and it becomes difficult to track any "identical" liquid structure.

Finally, LSFM also gives the opportunity for sizing of structures, e.g. droplets, which is presented for the
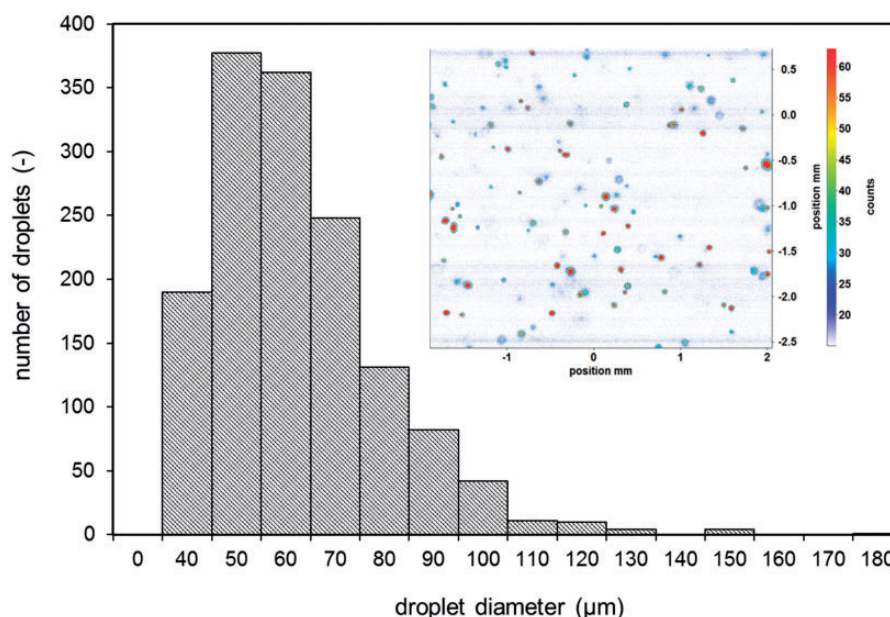
Figure 10. Histogram of valuated droplet sizes and example of LSFM image of the hollow-cone water spray. The pressure of injection was 80 bar and the measurement position was 120 mm below the injector.

water spray in a distance of 120 mm from the nozzle. In Figure 10, a histogram of evaluated droplet sizes is presented together with a single shot LSFM image. The evaluation was conducted using a Matlab routine (in-house script). About 3500 droplets were collected (50 images). Only droplets with sphericity of 1.0–1.1 were processed. The droplets in the background (low signal, they appear blurred) were sorted out. Droplets at the image boundary or that tend to collide were also rejected. Altogether, about 1500 droplets were evaluated. The class intervals (bins) were 10 μm and the average droplet size was 67 μm. It can be concluded, that the LSFM technique has the capability to study the secondary breakup of the droplets as well as droplet evaporation behavior or even droplet interactions (collisions and coalescence) also for small droplets of technically relevant atomizers.

Conclusions

LSFM imaging has been applied for the study of an atomizing water spray generated by a pressure swirl atomizer and for a multi-jet DISI spray. This attempt, which has not been fully investigated in the past, is successfully achieved here thanks to:

- The recent development of highly performing long-distance microscope objectives where the limit of image resolution was here due to the pixel resolution, and not by the imaging system.
- The use of highly sensitive sCMOS cameras (∼55% quantum efficiency) allows image intensifiers to be avoided, thus optimizing the full pixel array (2560 × 2160) of the sensor.
- The use of a fluorescent dye with good quantum yield in water and ethanol in order to generate a strong fluorescence signal even with a standard 532 nm excitation wavelength.

It is observed that the LSFM provides a higher image contrast than the back detection line of sight. In addition, it offers the possibility to clearly observe the nozzle orifice itself, which is hardly achievable with shadowgraph images. Finally, for the study of the near-nozzle region, where evaporation is not yet occurred, the fluorescence signal remains a faithful signature of the liquid bodies themselves. This appears not to be the case for the Mie-scattering detection, where microscopic representation of the spray is questionable on a light sheet configuration. Series of LSFM spray images can be of great importance for better understanding the atomization process occurring in the spray formation region and can be very attractive due to the simplicity of its optical arrangement and fairly low cost. Such analysis is significant to understand the primary

structure of the injected liquid at the nozzle tip, the breakup processes occurring in the spray formation region as well as the droplet dynamics in the spray region.

References

1. Huisken J, Swoger J, Del Bene F, et al. Optical sectioning deep inside live embryos by selective plane illumination microscopy. *Science* 2004; 305: 1007–1009.
2. Huisken J and Stainier DYR. Selective plane illumination microscopy techniques in developmental biology. *Development* 2009; 136: 1963–1975.
3. Stelzer EHK. Light-sheet fluorescence microscopy for quantitative biology. *Nature Methods* 2015; 12: 23–26.
4. Editorial. Method of the Year 2014. *Nature Methods* 2015; 12: 1–1.
5. Melton LA and Verdieck JF. Vapor/liquid visualization in fuel sprays. *Combust Sci Technol* 1985; 42: 217–222.
6. Berrocal E, Kristensson E, Richter M, et al. Application of structured illumination for multiple scattering suppression in planar laser imaging of dense sprays. *Optics Express* 2008; 16: 17870–17881.
7. Kristensson E, Berrocal E, Richter M, et al. High-speed structured planar laser illumination for contrast improvement of two-phase flow images. *Optics Letters* 2008; 33: 2752–2754.
8. Wellander R, Berrocal E, Kristensson E, et al. Three-dimensional measurement of the local extinction coefficient in a dense spray. *Meas Sci Technol* 2011; 22: 1–15.
9. Grosshans H, Kristensson E, Szász R-Z, et al. Prediction and measurement of the local extinction coefficient in sprays for 3D simulation/experiment data comparison. *Int J Multiphase Flow* 2015; 72: 218–232.
10. Kristensson E, Berrocal E, Richter M, et al. Nanosecond structured laser illumination planar imaging for single-shot imaging of dense sprays. *Atom Sprays* 2010; 20: 337–343.

11. Kristensson E, Berrocal E and Aldén M. Two-pulse structured illumination imaging. *Optics Letters* 2014; 39: 2584–2587.

12. Crua, C, Shoba T, Heikal MR, et al. High-speed microscopic imaging of the initial stage of diesel spray formation and primary breakup. *SAE Technical Paper* 2010-01-2247.

13. Crua C, de Sercey G and Heikal MR. Dropsizing of near-nozzle diesel and RME sprays by microscopic imaging 2012. In: *12th ICLASS*, Heidelberg, Germany, 2–6 September 2012.

14. Crua C, Heikal MR and Gold MR. Microscopic imaging of the initial stage of diesel spray formation. *Fuel* 2015; 157: 140–150.

15. Zhang X, Zhang J and Liu L. Fluorescence properties of twenty fluorescein derivatives: Lifetime, quantum yield, absorption and emission spectra. *J Fluoresc* 2014; 24: 819–826.

16. Trost J, Zigan L and Leipertz A. Quantitative vapor temperature imaging in DISI-sprays at elevated pressures and temperatures using two-line excitation laser-induced fluorescence. *Proc Combust Inst* 2013; 34: 3645–3652.

17. Storch M, Lind S, Will S, et al. Influence of ethanol admixture on the determination of equivalence ratios in DISI engines by laser-induced fluorescence. *Appl Optics* 2016; 55: 8532–8540.

18. Storch M, Mishra YN, Koegl M, et al. Two-phase SLIPI for instantaneous LIF and Mie imaging of transient fuel sprays. *Opt Lett* 2016; 41: 5422–5425.

19. Heldmann M, Bornschlegel S and Wensing M. Investigation of jet-to-jet interaction in sprays for DISI engines. SAE 2015-01-1899 (JSAE 20159261), 2015.

20. Zigan L, Shi JM, Krotow I, et al. Fuel property and fuel temperature effects on internal nozzle flow, atomization and cyclic spray fluctuations of a DISI-injector. *Int J Engine Res* 2013; 14: 543–556.